JOURNAL OF GEOPHYSICAL RESEARCH, VOL. 87, NO. B13, PAGES 10,579-10,597, DECEMBER 10, 1982

WAVEFORMS AND SPECTRA OF PRESHOCKS AND AFTERSHOCKS OF THE 1979 IMPERIAL VALLEY, CALIFORNIA, EARTHQUAKE: EVIDENCE FOR FAULT HETEROGENEITY?

James C. Pechmann and Hiroo Kanamori

Seismological Laboratory, California Institute of Technology, Pasadena, California 91125

Abstract. We have compared digitally-recorded waveforms of M_L 2.0-2.8 earthquakes that occurred in two small areas along the Imperial fault before and after it broke in the M_L 6.6 Imperial Valley earthquake on October 15, 1979. Eight preshocks (1977-1979) from a $4^1/2$ by $1^1/2$ km area centered 4 km SE of the mainshock epicenter have strikingly similar waveforms over the entire record length (~30 s), with an average peak cross correlation between seismograms of 0.74. The seismograms are well correlated at frequencies up to at least 4 Hz. This implies similar source mechanisms and hypocenters within $^1/4$ of the 4-Hz wavelengths, i.e., <200-400 m. Five aftershocks from the same area show an average peak cross correlation between seismograms of only 0.23. Any associated changes in mechanism must be small because they are not reflected in the first motion data. Analysis of frequency content of these events using bandpass-filtering techniques showed no systematic temporal changes in spectral shape. Ten preshocks and 24 aftershocks from a $1^1/2$ by 2 km source area centered along the fault 16 km NW of the mainshock epicenter were also studied. First motion data suggest that all of the aftershocks and a swarm of six preshocks on December 7-9, 1978, were associated with the main fault but that four earlier preshocks were not. The six preshocks on December 7-9, 1978, were tightly clustered, as evidenced by the strong similarity of the waveforms (most peak cross correlations >0.6). During this swarm the 8- to 16-Hz spectral amplitude increased relative to the 1- to 2-Hz spectral amplitude over the whole record length by about a factor of 3, suggesting a systematic increase in stress drop. Groups of like events are also present among the aftershocks in this data set. The average peak correlation for pairs of aftershocks, 0.43, is almost the same as that for pairs of preshocks, 0.45, if all 10 preshocks are included. However, several sources appear to have been active simultaneously during the aftershock period so that no more than two to three consecutive aftershocks have maximum cross correlations >0.6. The highly localized sources characterized by waveform similarity may represent fault asperities or clusters of asperities. Our observations are consistent with a decrease in the number of these asperities as the weaker ones fail under increasing stress during the intervals between large earthquakes.

Introduction

Seismological and geological observations suggest that the mechanical properties of a fault zone are not homogeneous. Inspection of active and inactive fault zones in outcrops and in tunnels has shown them to be very heterogeneous in geometry, pore fluid pressure, and fault zone material [Wu, 1980]. Surface rupture accompanying large earthquakes is usually complex, with irregular variations in displacement along the fault [Das and Aki, 1977; Aki, 1979]. Seismic body waves radiated by large events are also complex and are usually interpreted using multiple event source models [Imamura, 1937, p. 267; Wyss and Brune, 1967; Rial, 1978; Kanamori and Stewart, 1978]. Detailed modeling of short-period waveforms suggests that much of the higher-frequency energy comes from small, high stress drop areas on the fault plane [Cipar, 1981; Ebel, 1981; Wallace et al., 1981]. The highly randomized nature of strong motion accelerograms implies large variations in effective stress during fault rupture [Housner, 1955; Nur, 1978].

Those parts of a fault with higher than average strength, commonly called asperities, may play an important role in the processes leading up to large-scale failure. Jones and Molnar [1979] proposed that foreshocks represented accelerating failure of asperities due to concentration of stress on the unbroken asperities. Kanamori [1981] and Mikumo and Miyatake [1982] were able to explain with simple asperity models many of the longer-term spatio-temporal seismicity patterns which commonly precede major earthquakes. These include precursory swarms, quiescence, doughnut patterns, and foreshocks. Although the success of simple asperity models in explaining observed seismicity patterns is encouraging, the patterns themselves are too varied to be used reliably for earthquake prediction or to provide a good test of the models. Thus, it is desirable to examine other consequences of the models.

The key elements of asperity models that relate small earthquakes to large-scale seismic strain accumulation and release, such as those proposed by Kanamori [1981] and Mikumo and Miyatake [1982], are (1) fault surfaces are held together by a number of strong points or asperities, (2) weaker asperities fail during small earthquakes as tectonic stress increases, thereby transferring more stress to the remaining asperities, and (3) the fault becomes unstable when most, but not necessarily all, of the asperities have broken [Das and Aki, 1977; Brune, 1979]. These assumptions lead to two predictions about foreshocks: (1) On the average, stress drops of foreshocks should be higher than stress drops of previous events from the area, assuming that stress drop is proportional to tectonic stress, and (2) the foreshocks should be concentrated along strong asperities and hence should occur as groups of

Paper number 2B1360.
0148-0227/82/002B-1360$05.00

events with very similar locations and focal mechanisms and thus very similar waveforms. The extent to which this will occur depends on the nature of the asperities. In this paper, we will use the term asperity model to refer to a specific family of models in which concentration of stress on the stronger parts of the fault is an important factor controlling the locations and source parameters of small earthquakes.

Efforts to test the first of the predictions outlined above have produced mixed results [Reyners, 1981]. This may be due to problems with the data rather than with the model. In the numerical simulations of Kanamori [1981] a ratio of 4 of the stress drop of foreshocks to other events is enough to produce the observed seismicity patterns. Since frequency content depends on many other factors such as rupture velocity and direction, near-source velocity structure, and focal mechanism, it may be difficult to detect temporal changes in stress drop of this magnitude, especially since data from only one or two stations is usually available. Furthermore, changes in anelastic attenuation near the fault caused by opening or closing of cracks or movement of pore fluids may complicate the situation.

Relatively few studies have been made of waveforms of foreshocks. Ishida and Kanamori [1978] observed that seismograms of five events that occurred in the epicentral region of the 1971 San Fernando earthquake during the 2 years before this earthquake were remarkably similar. Frankel [1981b] found that six out of seven preshocks to a magnitude 4.8 earthquake in the Virgin Islands occurred as pairs of events with very similar waveforms. Waveform similarity, however, does not appear to be unique to foreshocks, and not all foreshocks exhibit waveform similarity. Hamaguchi and Hasegawa [1975] noted that many of the aftershocks of the 1968 Tokachi-Oki earthquake had similar waveforms and concluded that these similar events occurred at approximately the same location under the same mechanical conditions. Groups of events with similar waveforms that are not closely associated in time with major earthquakes have been reported by Stauder and Ryall [1967] in central Nevada and by Geller and Mueller [1980] and Spieth and Geller [1981] along the San Andreas fault in central California. Unpublished data collected by Kanamori show that waveforms of small earthquakes from the southeast portion of the Anza gap on the San Jacinto fault in California [Thatcher et al., 1975] have been nearly the same from 1933 to the present. Waveforms of foreshocks to the 1952 Kern County earthquake, in contrast to the San Fernando foreshocks, differed significantly from event to event [Ishida and Kanamori, 1980]. The seismograms for two foreshocks to the 1966 Parkfield earthquake shown in Figure 2 of Bakun and McEvilly [1979] do not look very much alike, nor do the two foreshocks to the 1975 Oroville earthquake shown in Figure 5 of the same paper. Tsujiura [1979a] reported that seven swarms in the Kanto district of Japan were characterized by similarity of waveforms but that the waveforms of foreshocks to the 1978 Izu-Oshima earthquake showed substantial variation. The Izu-Oshima earthquake, however, had a very complicated rupture zone, and there is a strong possibility that many of the foreshocks were not associated with the main fault [Tsumura et al., 1978]. Furthermore, Tsujiura [1979b] notes that during one of the stronger swarms studied, the percentage of events in groups with similar waveforms decreased after the largest event (M 5.5) occurred. This suggests that even in hindsight an a priori distinction between preshocks, swarms, and aftershocks is not necessarily straightforward.

It seems clear that even if the asperity model is correct, the number of foreshocks and the degree of waveform similarity among them will depend on the number, strength, and distribution of asperities involved. Furthermore, it is possible that failure of weaker asperities could produce small groups of similar events at any time. These complications must be considered when investigating the asperity model using waveforms.

In this study we test the predictions of the asperity model regarding temporal variations of waveform and spectra of small earthquakes along major faults. The data we use are digitally-recorded seismograms from the CEDAR system [Johnson, 1979] of preshocks and aftershocks of the October 15, 1979, M_L (local magnitude) 6.6 Imperial Valley earthquake. The low detection threshold and high location resolution of CEDAR and the California Institute of Technology/U.S. Geological Survey southern California array enables comparison of many events from small (<5 km) source regions during different time periods, which was not possible in most previous studies of waveforms and spectra. Since the CEDAR system has only been in operation since January 1, 1977, the time span of observations is rather short compared to the time between the last two major earthquakes along the Imperial fault (39 years). Nevertheless, if we consider these aftershocks and preshocks to be representative of the beginning and end of the seismic cycle, respectively, then some information regarding longer-term temporal variations can be inferred. We find some evidence to support both predictions of the asperity model outlined above. However, on the basis of this study it appears that waveform is a more reliable indicator of stress conditions along faults than is frequency content.

Selection of Events and Stations

The 1979 Imperial Valley earthquake was accompanied by right-lateral surface faulting along the northernmost 30 km of the Imperial fault (Figure 1), with coseismic displacements exceeding 40 cm in some places (K. Sieh, written communication, 1979). Along the northern half of the rupture zone, vertical slip (NE side down) of up to 30 cm also occurred. A segment of the Brawley fault, east of the Imperial fault, also broke during the earthquake. The 1979 faulting was very similar to the faulting which occurred in 1940 along the northern part of the Imperial fault. However, the 1940 earthquake also produced very large right-lateral offsets (up to 5.8 m) on the southern half of the fault [Richter, 1958, pp. 489-491].

The mainshock epicenter of Chavez et al. [1980], calculated using stations in both the

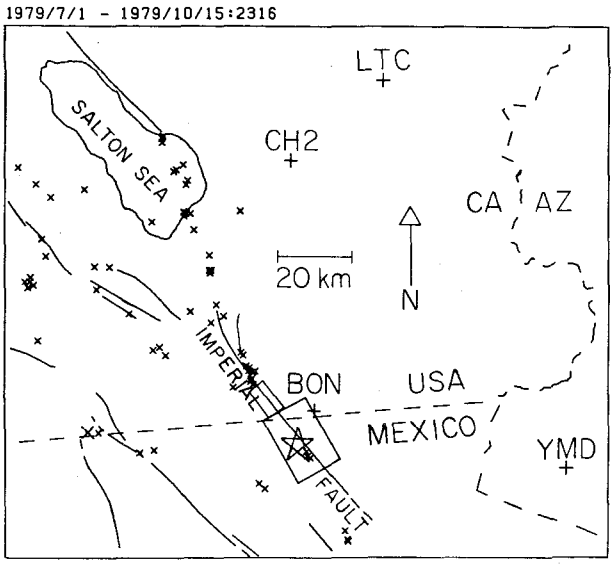

Fig. 1. Map of Imperial Valley and surrounding area showing major faults [Jennings et al., 1975], key seismographic stations, and all well-located epicenters (epicentral error of less than 5 km) from the preliminary Caltech-USGS catalog for the period July 1, 1979, to October 15, 1979, 2316 (the time of the M_L 6.6 mainshock). The small crosses are $M_L<3.0$ events and the large crosses are events with $3.0<M_L<4.0$. The large star is the preliminary mainshock epicenter. The solid boxes show the areas for which relocations were done (Figures 2 and 3). The north-striking fault near the northern end of the Imperial fault is the Brawley fault [Sharp, 1976]. The northwest-striking fault on the northeast side of the Salton Sea is the San Andreas fault.

United States and Mexico, is located in Mexico about 8 km SE of the nearest surface faulting. Figure 1 shows the Caltech-USGS preliminary epicenter, which is slightly too far to the south, together with all well-located (epicentral error of less than 5 km) earthquakes in the area for the $3^1/2$ months preceding the mainshock. This time period was reported by Johnson and Hutton [1980] to be anomalously quiet. Note that there are only three events during this period within ~15 km of the impending mainshock epicenter. This pattern of quiescence over a large part of the fault, accompanied by clustering near the future hypocenter, is often observed before large earthquakes [Kanamori, 1981]. The aftershocks of the 1979 earthquake were concentrated at the northern end of the fault, but there was also significant aftershock activity along the central part of the rupture zone [Johnson and Hutton, 1980].

In looking for temporal changes, it is desirable to minimize changes in the source-receiver geometry and to compare events of roughly the same size. We therefore decided to select two small sections of the fault for study and to look at all $M_L \geq 2.0$ events from these areas. We chose this size range because most of the events in the regions of interest were less than magnitude 3 and the estimated uniform detection threshold in the border region is magnitude 2 [Johnson, 1979].

One place that is clearly of interest is the spot near the mainshock epicenter where three events occurred during the quiet period preceding the mainshock. In order to find previous events and aftershocks from this area, we relocated all $M_L \geq 2.0$ events from the box surrounding the epicenter in Figure 1. Relocations were done relative to the hypocenter of Chavez et al. [1980] using the master event technique [Johnson and Hadley, 1976] with the computer program HYPO71 [Lee and Lahr, 1975]. The velocity model used was the same as that used by Chavez et al. [1980] (Table 1). It is a layered approximation to the model derived by McMechan and Mooney [1980] for the southern Imperial Valley on the basis of synthetic seismogram modeling of refraction data [Fuis et al., 1980]. The model matches P-wave travel times from these earthquakes quite well out to ~120 km distance. Arrival time picks were made by the Caltech-USGS staff as part of the routine data processing. Fifteen stations were used in the relocations, all in the United States and all at epicentral distances of less than 90 km. The absolute value of the average travel time residual was 0.08 s or less at all these stations.

Figure 2 shows relocations of earthquakes from the time of the installation of the Imperial Valley array in July 1973 through July 1980. Relocated epicenters tend to be a few kilometers north and east of the catalog epicenters, consistent with the approximately 3 km north-northeastward shift of the mainshock location of Chavez et al. [1980] relative to the Caltech-USGS mainshock location. The relocated epicenters are more tightly aligned along the Imperial fault than those in the catalog. The depths for the relocated hypocenters are all less than 12 km, whereas many of the catalog depths are deeper than this, down to 23 km. This is because the standard locations are determined with an average southern California velocity model that does not include the thick layer of low-velocity sedimentary rocks at the surface in the Imperial Valley. The dashed box in Figure 2 shows the source area that we chose to investigate, $4^1/2$ km by $1^1/2$ km. The box

TABLE 1. Imperial Valley Crustal Velocity Model

P-Wave Velocity of Layer, km/s	Depth to Top of Layer, km
2.00	0.0
2.40	0.5
2.80	1.0
3.45	2.0
4.10	3.0
4.75	4.0
5.45	5.0
5.80	6.0
6.75	10.0
7.05	10.5
7.20	11.0

From Chavez et al. [1980]. Based on refraction studies by Fuis et al. [1980].

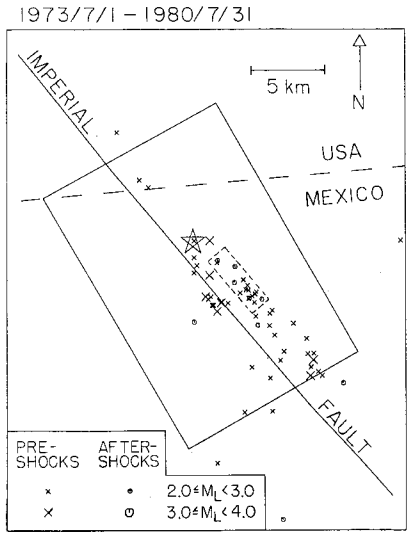

Fig. 2. Relocated epicenters for all $M_L \geq 2.0$ events in the solid box from July 1, 1973, to July 31, 1980. The mainshock location of Chavez et al. [1980] (star) was used as a master event for the relocations. The dashed box encloses the events selected for study (Table 2).

includes the three preshocks shown in Figure 1, five additional preshocks for which digital data are available, and five aftershocks (Table 2). Local magnitudes range from 2.2 to 2.5 for the preshocks and from 2.0 to 2.8 for the aftershocks. The calculated depths, although not well constrained, are all in the range 7-10 km.

A second region of interest is shown by the small solid box just north of the border in Figure 1. We decided to select a cluster of events for study from this section of fault because (1) coseismic and postseismic surface displacements were largest there, (2) strong motion modeling by Hartzell and Helmberger [1982] and LeBras [1981] suggests large subsurface slip in this area, up to 2.5 m, and (3) this section of fault straddles the boundary between the Brawley seismic zone to the NW and a 10-15 km nearly aseismic zone along the Mexican border, which separates the 1979 mainshock epicenter from the 1940 epicenter [Johnson and Hutton, 1980]. The relocation procedure for this box was the same as for the box to the south except that the master event used was a well-located M_L 2.7 preshock on December 7, 1978, from the NW end of the box. Sixteen stations were used, all at distances less than 90 km. The absolute value of the average travel time residual for these master event relocations was 0.05 s or less at 15 out of the 16 stations. The average residual for the other station was 0.20 s, probably because the first arrival was missed in some cases.

Figure 3 shows relocated epicenters of all $M_L \geq 2.0$ events from this area for the period January 1977 through March 1981. The relocated epicenters are again more tightly grouped along the fault trace, and many of the locations are several kilometers shallower than those in the catalog because of the different velocity model used. Because most of the preshocks which we relocated were near the NW edge of the box, we selected the subset of events within the $1\frac{1}{2}$ by 2 km dashed box (Figure 3) for study. These events, 10 preshocks and 30 aftershocks, are listed in Table 3. Six of the aftershocks could not be used, either because seismic waves from another aftershock were arriving concurrently or because CEDAR data were not available. The magnitude range for both the preshocks and the useable aftershocks is 2.0-2.8. The depths of most of the events are 9-11 km. In general, these hypocenters are more accurate than those from south of the border (Table 2 and Figure 2) because the stations are closer and better distributed in azimuth.

Selection of stations for waveform and spectral studies was complicated by clipping of some of the signals during telemetry and by changes in instrumentation during the time period of interest. Changes in instrumentation implemented at most of the southern Imperial

TABLE 2. Relocated Hypocenters in Dashed Box in Figure 2

Date	Time	Latitude	Longitude	Depth,km	M_L
May 13, 1974	1744:48.58	32°36.77′	115°15.87′	9.4	2.2 *
April 9, 1976	2347:52.46	32°36.73′	115°16.56′	9.5	2.2 *
Aug. 28, 1977	1607:40.62	32°36.85′	115°16.31′	9.4	2.4
Sept. 15, 1977	2016:56.41	32°36.40′	115°15.95′	9.1	2.4
June 8, 1978	0015:31.49	32°36.69′	115°15.93′	9.3	2.4
Aug. 4, 1978	0059:58.29	32°37.01′	115°16.24′	9.5	2.4
May 11, 1979	1924:32.78	32°36.84′	115°16.20′	9.6	2.4
Aug. 7, 1979	1637:32.59	32°37.21′	115°16.42′	9.9	2.5
Aug. 25, 1979	0440:46.01	32°36.54′	115°16.19′	9.6	2.5
Sept. 10, 1979	1527:00.35	32°36.72′	115°15.93′	9.4	2.2
Oct. 17, 1979	1106:50.72	32°37.69′	115°16.78′	8.7	2.0
Oct. 27, 1979	2154:40.78	32°37.12′	115°16.81′	7.6	2.8
Nov. 10, 1979	2035:42.97	32°37.91′	115°17.53′	9.5	2.6
Dec. 17, 1979	0918:17.33	32°36.56′	115°16.17′	10.0	2.5
May 21, 1980	0853:55.94	32°36.52′	115°15.64′	9.2	2.0

* Digital data unavailable

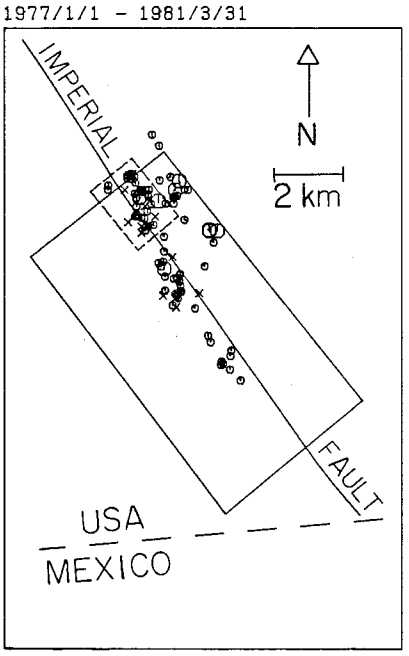

Fig. 3. Relocated epicenters for all $M_L \geq 2.0$ events in the solid box from January 1, 1977, to March 31, 1981. The master event used was an M_L 2.7 preshock on December 7, 1978, located within the area selected for detailed study (dashed box). Magnitude key same as in Figure 2.

Valley stations on July 17, 1979, unfortunately rendered them unuseable for our purposes. At this time, Airpax discriminators were replaced with modified J-101 discriminators equipped with antialiasing filters. Since the Airpax discriminators showed considerable variation in frequency response from one unit to another (C. Koesterer, personal communication, 1980), it would have been difficult to correct for the change by digital filtering. Modified J-101 discriminators were also installed at stations in the southeastern Mojave desert several months earlier. Some of these stations, however, were previously equipped with unmodified J-101 discriminators, for which the response is well known. Using analytic expressions for the modified and unmodified system responses from Archambeau [1979], we designed a time-domain digital filter to mimic the instrumentation change. Figure 4 shows a test of this filter. The top seismogram in each group was recorded using the unmodified instrumentation, and the bottom one was recorded using the modified instrumentation. The second trace is the digitally filtered version of the first trace, and in both cases it resembles the third trace quite closely. This procedure is valid as long as the original signal does not contain significant energy above 25 Hz, the Nyquist frequency of CEDAR.

Good recordings of most of the events in Tables 2 and 3 were available at three stations for which it was possible to correct for the instrumentation change: YMD, CH2, and LTC (Figure 1). The standardized frequency response of these instruments is reasonably broadband, within a factor of 4 of the peak amplitude response (near 7 Hz) over the range 1-16 Hz [Archambeau, 1979]. These stations were used for the studies of waveform and spectra discussed in the following sections.

Waveforms and Focal Mechanisms

Seismograms for events in the dashed box in Figure 2 (Table 2) are shown in Figures 5, 6, and 7. The change in instrumentation has been corrected for, and the instrument response has been deconvolved in the passband 1-16 Hz. Horizontal lines separate the preshocks from the aftershocks. At all three stations, the preshocks show remarkable similarity in waveform and in relative arrival times and amplitudes of various phases over the entire record length (~30 s). Because the character of the record is controlled by scattering from velocity heterogeneities in the crust, the similarity of the waveforms implies similar source mechanisms and hypocenters within $1/4$ of the shortest wavelength to which the similarity extends [Geller and Mueller, 1980]. Available first motion data for the preshocks support the inference of similar source mechanisms (Figure 8), but by themselves are inadequate to constrain the solutions. However, SV/P amplitude ratios for these preshocks at station BON ($\Delta \simeq 9$ km), together with the available first motions, suggest right-lateral strike-slip on a NW-striking plane or left-lateral strike-slip on a NE-striking plane (C. Jones, personal communication, 1980).

Seismograms of preshocks from this area are much more similar to one another at each station than seismograms of aftershocks. To demonstrate this, we cross correlated the seismograms. The normalized cross-correlation function $c_{xy}(m)$ for two real time series x and y of length N is given by

$$c_{xy}(m) = \frac{[1/(N-|m|)] \sum_{n} x(n)y(n+m) - \overline{x(n)}\ \overline{y(n+m)}}{\sqrt{\overline{x^2(n)} - \overline{x(n)}^2}\sqrt{\overline{y^2(n+m)} - \overline{y(n+m)}^2}}$$

where the bar indicates the mean

$$\overline{x(n)} = \frac{1}{N-|m|} \sum_{n} x(n)$$

and the summation is from n=0 to n=N-m-1 for $m \geq 0$ and from n=|m| to n=N-1 for $m<0$. The maximum of $c_{xy}(m)$ for $|m| \leq N/4$ for each pair of consecutive events is plotted versus time in Figure 9. These graphs show clear changes at the time of the mainshock, indicated by the vertical bar. Figure 10 shows for all possible event pairs the mean of the maximum $c_{xy}(m)$ values calculated for the three different stations. Each mean peak correlation is represented by a circle, where the radius of the circle is proportional to the mean peak correlation value. Values greater than or equal to 0.6 are shown by open circles and smaller values are shown by solid circles. It is evident from this figure that the preshocks display much greater coherency in waveform than

TABLE 3. Relocated Hypocenters in Dashed Box in Figure 3

Date	Time	Latitude	Longitude	Depth,km	M_L	
Dec. 14, 1977	0317:27.72	32°45.49′	115°25.75′	9.0	2.0	
Feb. 24, 1978	0636:38.37	32°44.93′	115°25.44′	4.4	2.4	
Feb. 24, 1978	0638:10.06	32°44.83′	115°25.44′	9.4	2.1	
Feb. 24, 1978	0758:27.44	32°44.99′	115°25.69′	10.1	2.0	
Dec. 7, 1978	2213:22.18	32°45.49′	115°25.44′	10.2	2.7	+
Dec. 8, 1978	0202:00.93	32°45.08′	115°25.19′	10.2	2.4	
Dec. 8, 1978	0838:23.01	32°45.74′	115°25.61′	11.2	2.8	
Dec. 8, 1978	0842:18.57	32°45.49′	115°25.44′	10.1	2.6	
Dec. 8, 1978	0847:48.47	32°45.49′	115°25.44′	10.4	2.7	
Dec. 9, 1978	0217:41.62	32°45.24′	115°25.38′	10.9	2.8	
Oct. 16, 1979	0048:03.41	32°45.32′	115°25.13′	10.1	3.1	**
Oct. 16, 1979	0953:47.57	32°45.49′	115°26.07′	10.1	2.7	*
Oct. 16, 1979	1703:33.04	32°45.56′	115°26.06′	9.6	2.5	
Oct. 16, 1979	1916:51.95	32°45.60′	115°25.56′	10.1	2.6	
Oct. 17, 1979	0506:42.96	32°45.05′	115°25.39′	10.1	2.1	
Oct. 17, 1979	0937:59.16	32°45.16′	115°25.34′	10.1	2.7	
Oct. 17, 1979	2307:03.62	32°45.28′	115°25.00′	10.6	2.2	
Oct. 19, 1979	0310:44.19	32°45.43′	115°25.57′	10.1	2.6	
Oct. 22, 1979	1922:27.44	32°45.67′	115°25.71′	10.1	2.2	
Oct. 24, 1979	0552:51.21	32°45.10′	115°25.53′	9.6	2.3	
Oct. 24, 1979	0619:04.68	32°45.69′	115°25.57′	10.1	2.7	**
Oct. 26, 1979	0911:16.68	32°45.39′	115°25.32′	10.9	2.5	
Oct. 28, 1979	0203:43.33	32°45.23′	115°25.54′	10.1	2.2	
Oct. 28, 1979	1621:31.41	32°45.46′	115°25.44′	10.2	2.0	**
Oct. 29, 1979	0204:53.55	32°45.49′	115°25.30′	9.6	2.3	**
Oct. 29, 1979	0647:55.70	32°45.49′	115°25.46′	10.1	2.7	
Oct. 30, 1979	2101:48.34	32°45.36′	115°25.54′	10.1	2.7	
Oct. 31, 1979	1708:34.17	32°45.08′	115°25.56′	10.8	2.3	
Nov. 2, 1979	2145:29.24	32°45.66′	115°25.63′	10.1	2.7	
Nov. 7, 1979	0200:54.77	32°44.95′	115°25.22′	10.1	2.4	
Nov. 7, 1979	1426:33.31	32°45.71′	115°25.70′	10.1	2.2	
Nov. 7, 1979	1433:22.70	32°45.73′	115°25.62′	10.1	2.2	
Nov. 9, 1979	2303:57.35	32°45.37′	115°25.48′	10.1	3.0	**
Nov. 10, 1979	0223:41.73	32°45.27′	115°25.26′	10.1	2.2	
Nov. 11, 1979	1532:45.66	32°45.42′	115°25.32′	10.2	2.7	
Nov. 11, 1979	1559:23.47	32°45.49′	115°25.31′	10.7	2.4	
Nov. 16, 1979	1435:04.95	32°44.93′	115°25.31′	9.1	2.4	
Nov. 19, 1979	1845:00.31	32°44.86′	115°25.37′	10.7	2.8	
Nov. 25, 1979	0856:31.20	32°45.47′	115°25.46′	10.1	2.1	
Feb. 25, 1981	2021:02.53	32°45.06′	115°25.44′	10.1	2.1	

\+ Master event
* Digital data unavailable
** Unuseable (multiple event)

do the aftershocks. The average peak correlation between preshocks (upper left box) is 0.74, whereas mean peak correlations between aftershocks (lower right box) are all small, less than 0.3, with an average value of only 0.23. The last two aftershocks correlate more strongly with the preshocks than the first three aftershocks do, but still not as strongly as most preshocks correlate with each other.

Examples of the cross-correlation function $c_{xy}(m)$ are shown in Figure 11. For well-correlated pairs of seismograms (top four examples), this function is sharply peaked near lag m=0 s. For poorly-correlated pairs of seismograms (bottom four examples), this peak is small or nonexistent. Thus, the maximum value of $c_{xy}(m)$ appears to be a robust measure of the similarity of two seismograms.

As mentioned above, the similarity of the preshock waveforms places a strong constraint on the maximum distance between the hypocenters. To help quantify this constraint, we cross correlated selected pairs of seismograms after bandpass filtering them in four one-octave passbands. Figure 12 shows cross correlations between filtered seismograms for a pair of preshocks (left) and a pair of aftershocks (right). The peaks of these cross-correlation functions are well above the noise for well-correlated events, such as the example on the left in this figure. The peak cross correlations between filtered traces are shown in Figure 13 for the event pairs in Figure 12 and four other pairs, including the least well-correlated pair of preshocks (June 8, 1978; August 4, 1978). Peak cross correlations for the

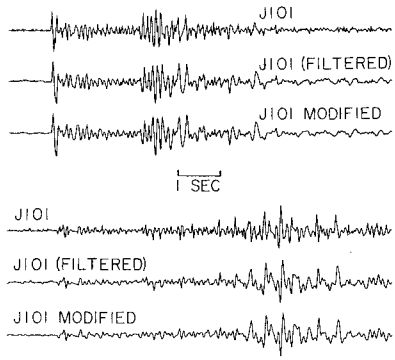

Fig. 4. Test of digital filter to compensate for change of instrumentation. Traces labeled J-101 were recorded through J-101 discriminators, and those labeled J-101 modified were recorded through modified J-101 discriminators. Traces labeled J-101 (filtered) were recorded through J-101 discriminators and then filtered with a digital filter that approximates the modifications made to the J-101. The examples shown are from an M_L 1.8 event on May 26, 1978, near San Gorgonio Pass. Top records are from station WWR (Δ=10 km), and bottom records are from station RMR (Δ=34 km).

unfiltered, deconvolved seismograms are shown for reference by the solid symbols at the left of each graph. The preshocks (top four graphs) are well correlated (peak correlations generally $\geq$0.6) up through at least the 2-4 Hz frequency band, whereas the aftershocks shown (bottom two graphs) are not well correlated at any frequency. The near-source P-wave velocity is about 6 km/s (Tables 1 and 2) and the S-wave velocity is probably of the order of 3.4 km/s. At 4 Hz the wavelengths are therefore ~1500 m for P waves and

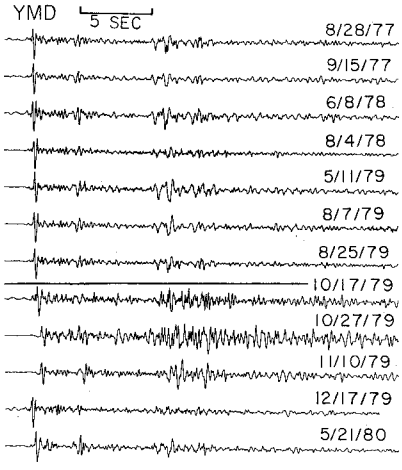

Fig. 5. Vertical component seismograms recorded at YMD (Δ≈68 km) for earthquakes from the dashed box in Figure 2. The instrument response has been deconvolved in the passband 1-16 Hz. Seismograms are plotted with the same maximum amplitude and positioned horizontally according to the recalculated origin times. Note that the preshock records are all very similar to one another, whereas the aftershocks show more variability.

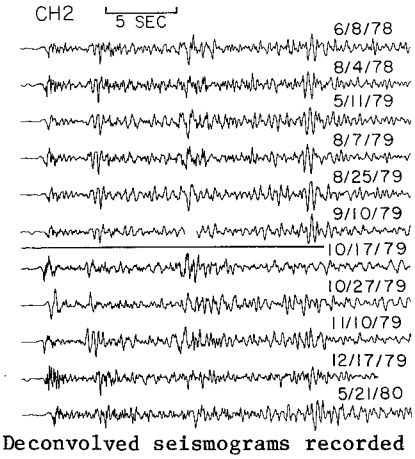

Fig.6. Deconvolved seismograms recorded at CH2 (Δ≈76 km). See Figure 5 for explanation. The data gap during the arrival of the third prominent phase from the September 10, 1979, event was caused by a disk drive failure.

~850 m for S waves. The similarity of preshock waveforms at these wavelengths and longer implies a maximum event separation of $^1/_4$ wavelength, approximately 200-400 m in this case.

The greater diversity of aftershock waveforms may be due to several factors such as greater variability in location, size, source mechanism, or pattern of stress release. However, there is very little difference in magnitude among these events (Table 2) and any changes in mechanism must be small because they are not reflected in the first motion data (Figure 8). The rupture time for magnitude 2-3 events is only a few tenths of a second long, so at the frequencies which dominate in these records, 3-6 Hz, the waveforms are insensitive to the details of the rupture and are instead dominated by the effects of structure and radiation pattern. It therefore appears that location is the dominant factor controlling the waveforms. This phenomenon is apparently below the resolution of even master

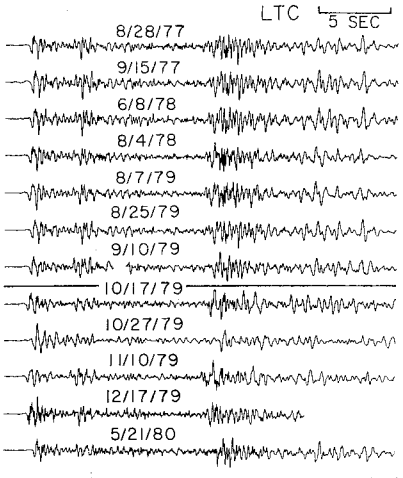

Fig. 7. Deconvolved seismograms recorded at LTC (Δ≈99 km). See Figure 5 for explanation. The data gap at ~7 s after arrival of the P wave from the September 10, 1979, event was caused by a disk drive failure.

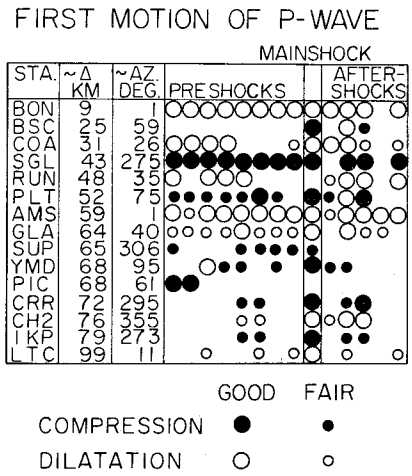

Fig. 8. First motion readings for events shown in Figures 5, 6, and 7.

event locations, because there is no obvious relationship between waveform and location within the study area.

Seismograms of events from within the dashed box of Figure 3 (Table 3) are shown in Figures 14 and 15. These are the original records except that some preshocks have been filtered to correct for the change in instrumentation. The numbers at the left of each seismogram show the maximum correlation between it and the seismogram above

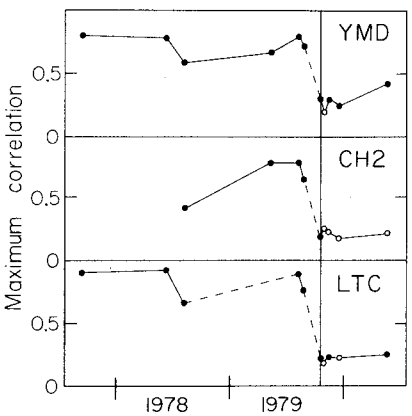

Fig. 9. Maximum cross correlation between each seismogram in Figures 5, 6, and 7 and the one directly above it, plotted as a function of time. The vertical bar marks the time of the mainshock. Solid circles are correlation coefficients corresponding to time lags where the phases are properly aligned. Open circles correspond to lags where the phases are not properly aligned, and hence represent upper limits to the maximum correlation in the sense that these numbers would decrease if the range of allowable lags ($\pm 1/4$ of the record length) was decreased. Thirty seconds of record were used in the cross-correlation calculations, except for the December 17, 1979, event. Dashed lines indicate intervals containing earthquakes that could not be included in this analysis because the records were unavailable or unuseable because of data gaps (see Figures 6 and 7).

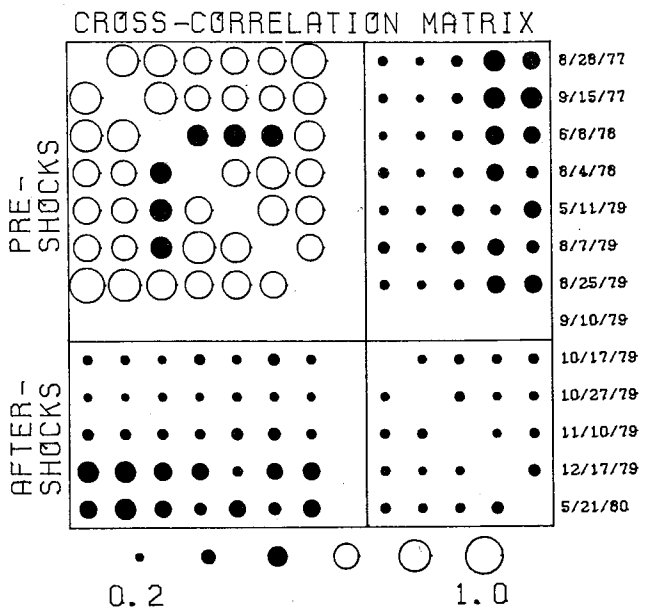

Fig. 10. The mean of the maximum cross correlations calculated for seismograms from YMD, CH2, and LTC for all possible pairs of events in Figures 5, 6, and 7. Each circle represents the mean peak correlation for the event pair corresponding to its position in the matrix. The radius of the circle is proportional to the correlation value. Circles representing values less than 0.6 are solid.

it. These numbers are plotted versus time in Figure 16, along with analogous peak correlations from station YMD. The mean peak correlations for all possible event pairs are shown in Figure 17.

The distinction between preshocks and aftershocks from this source region is not as obvious as for the events from near the epicenter in Figures 5-7. The average peak correlation for

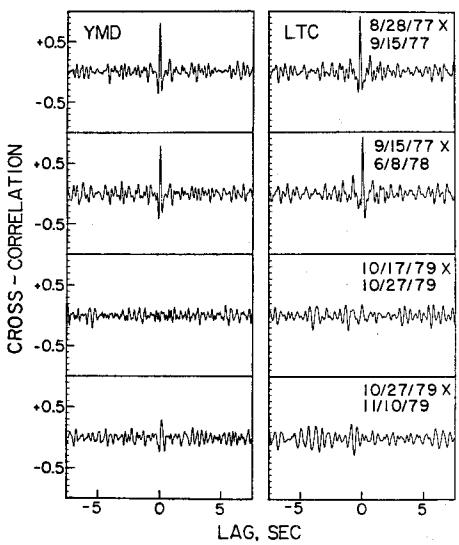

Fig. 11. Cross-correlation functions calculated from records at YMD (left) and LTC (right) for two pairs of preshocks (top two sets) and two pairs of aftershocks (bottom two sets).

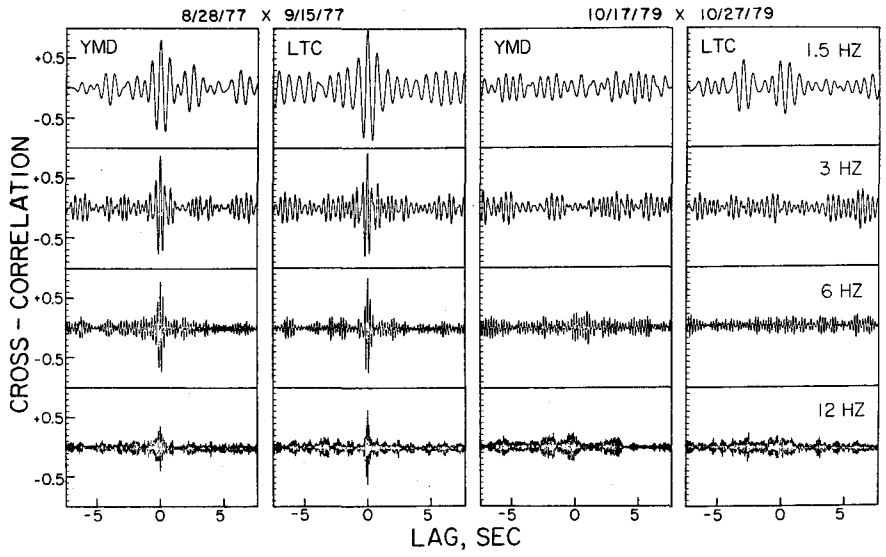

Fig. 12. Cross-correlation functions calculated after bandpass filtering the deconvolved seismograms in the passbands 1-2, 2-4, 4-8, and 8-16 Hz with third-order recursive Butterworth filters. Results are shown for stations YMD and LTC for a pair of preshocks (left two columns) and a pair of aftershocks (right two columns).

pairs of aftershocks (lower right box, Figure 17) is 0.43, nearly the same as the average for the preshocks, 0.45 (upper left box). Nevertheless, a close examination of the data suggests that differences exist between the preshock and aftershock periods. Three of the 10 preshocks occurred in a swarm on February 24, 1978, and six occurred in a swarm on December 7-9, 1978. The events within each swarm have very similar waveforms (most peak correlations ≥ 0.6), but different from those of the other swarm and the December 14, 1977, preshock (Figures 14-17). Sets of like events are also present within the aftershock sequence. However, after the mainshock it appears that several sources became active at once so that no more than two to three consecutive aftershocks have peak correlations ≥ 0.6.

Figure 18 shows the same data as Figure 17 except that the aftershocks are no longer chronological but have been rearranged to put similar events next to each other. This rearrangement effectively concentrates the larger circles near the diagonal. It is evident from Figure 18 that distinct groups of similar events exist among both the preshocks and the aftershocks, although there is some overlap between groups. The small boxes show one possible division of these earthquakes into groups. Only the preshock on December 14, 1977, and the aftershocks on December 16, 1979, 1703; November 16, 1979; and February 25, 1981, appear not to have close counterparts in this data set. At least two of the aftershocks have waveforms similar to those of the last preshocks to occur. These preshocks, the swarm on December 7-9, 1978, appear to be unique among these 34 events in terms of the number of consecutive earthquakes with similar waveforms.

The December 7-9, 1978, events are furthermore distinctive among the preshocks in that only these events have first motions consistent with

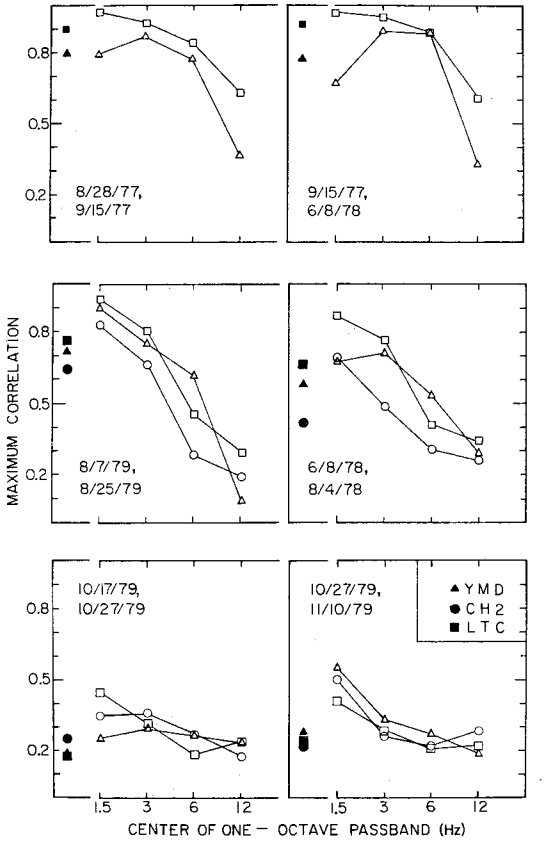

Fig. 13. Maximum cross correlations between filtered records (open symbols) for selected pairs of preshocks (top four graphs) and aftershocks (bottom two graphs), including the examples in Figure 12. Maximum cross correlations for the unfiltered, deconvolved (1-16 Hz) seismograms are shown for reference by the solid symbols at the left of each graph.

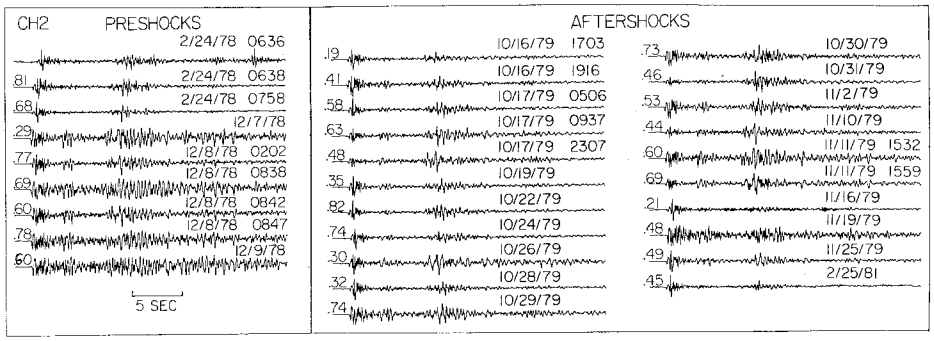

Fig. 14. Vertical component seismograms for earthquakes from dashed box in Figure 3, recorded at station CH2 ($\Delta \approx 60$ km). Seismograms are plotted with the same maximum amplitude and positioned horizontally within each column according to recalculated origin times. The numbers at the left of each seismogram show the maximum correlation between it and the seismogram above it. Thirty seconds of record were used in the cross-correlation calculations except for the February 24, 1978, 0636 event, where only 22 s could be used because of the arrival of a P wave from another event.

the mechanism of the mainshock (Figure 19). The December 7-9, 1978, preshocks and about half of the aftershocks have first motions consistent with pure right-lateral strike-slip motion on a vertical fault plane striking N40°W, the approximate local strike of the Imperial fault. These events are identified by asterisks in Figure 19. Figure 20 shows composite first motion plots for the two preshock swarms and also plots for two representative aftershocks. The contours in Figure 20 enclose the locus of positions for slip vectors corresponding to solutions with the minimum number of readings in error (zero for mechanisms a, c, and d and one for mechanism b). Figure 20d is typical of the aftershocks with asterisks in Figure 19 and Figure 20c is typical of the other aftershocks, which have different first motions at one or more of the following stations: COA, SGL, RUN, and GLA. Although the mechanism shown in Figure 20c, like the rest, is not well constrained, the data are consistent with right-lateral strike-slip motion on a plane deviating only about 15°-20° in strike from the average N40°W strike of the Imperial fault, as shown. It is therefore possible that all of the aftershocks in this set and the December 7-9, 1978, preshocks were associated with the main fault. On the other hand, the composite first motion plot for the February 24, 1978, swarm excludes mechanisms with shallowly-plunging slip vectors trending NW or SE. This is because of different first motions at SNR, SUP, and PLT (Figure 20a). Hence, these events and possibly the December 14, 1977, event may have occurred on a small nearby branch fault and not the main Imperial fault. If for this reason we exclude these preshocks from the data set, then the only preshocks remaining are the six in the December 7-9, 1978, swarm, which judging from their similarity in waveform must have occurred in a very tight cluster ($< \sim 1/2$ km).

The aftershock first motion plots (Figures 20c and 20d) suggest changes in fault strike of ~15°-20° within the region of the dashed box in Figure 3. No evidence for this was seen in the surface rupture (R. V. Sharp, personal communication, 1981). However, it is interesting to note that the slip model of Hartzell and Helmberger [1982] that best fits the strong motion data includes a change in fault strike from N37°W to N25°W (going north) at this point.

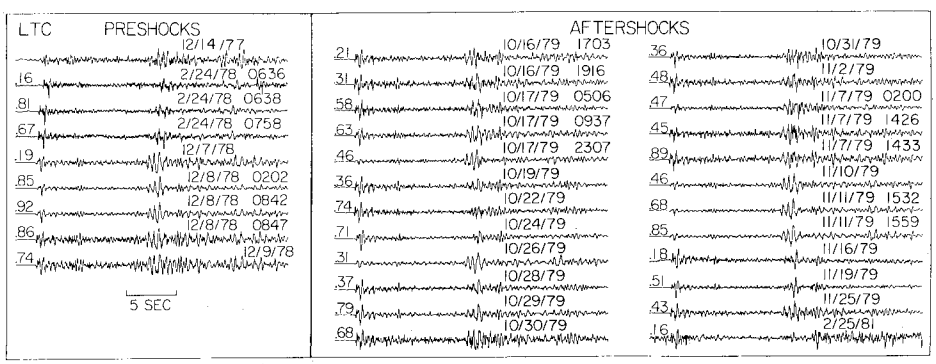

Fig. 15. Same as Figure 14, for station LTC ($\Delta \approx 88$ km). Thirty seconds of record were used in the cross correlations except for the following events: February 24, 1978, 0636 (22 s); February 24, 1978, 0758 (26 s); October 24, 1979 (29 s); October 28, 1979 (28 s).

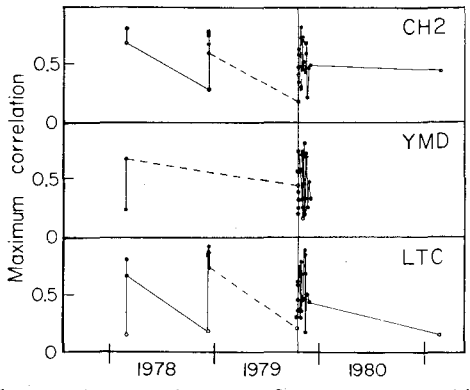

Fig. 16. Peak correlations from Figures 14 and 15 and analogous peak correlations from station YMD ($\Delta \approx 85$ km), plotted as a function of time. See Figure 9 for explanation. Dashed lines indicate intervals containing earthquakes that could not be included in this analysis because the records were unavailable or unuseable due to interference from other events.

They added this bend and others farther north to reproduce the P waveforms at the station nearest the fault. Their proposed change in fault strike fits the changes in aftershock first motions quite well except that there is no correlation between mechanism type and location within the box. This may be attributable to location error, since a comparison between waveforms and hypocenters suggests that location within the box is not well resolved by travel times.

True location appears to be the primary factor controlling the waveforms, as in the case of the events examined from near the mainshock epicenter. The classification of events by waveform in Figure 18 bears no relation to the magnitudes (Table 3). Radiation pattern may be

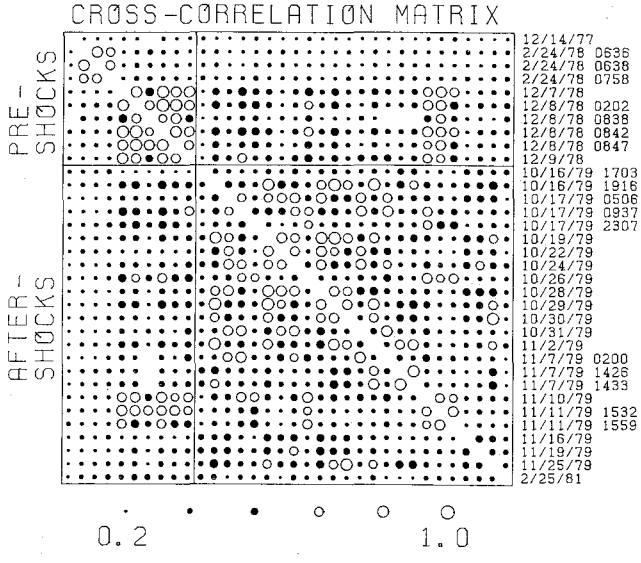

Fig. 17. The mean of the maximum cross correlations calculated for seismograms from YMD, CH2, and LTC for all possible event pairs in Figures 14 and 15. See Figure 10 for explanation.

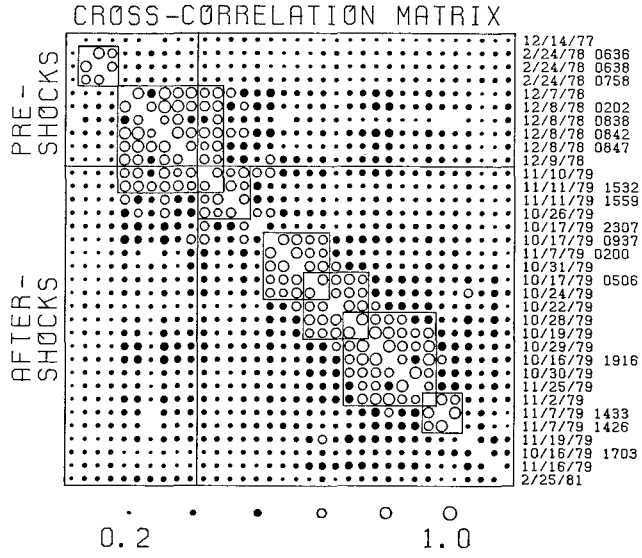

Fig. 18. Same as Figure 17 except that the order of the aftershocks in the matrix has been rearranged. Boxes show one possible way to classify the events according to waveform.

of some importance given that waveforms from the first four preshocks do not correlate well with waveforms from later events (Figure 17) and that the mechanisms for these four preshocks apparently differ significantly from the others (Figures 19 and 20). However, the pattern of first motions for the rest of the events is similar, and the differences which do exist are sometimes present within groups having nearly the same waveforms at YMD, CH2, and LTC (e.g., the events on October 19, 1979, and October 22, 1979). We therefore conclude that most families of similar events originate from small ($< \sim 1/2$ km), distinct source areas.

Spectral Analysis

Although the deconvolved records in Figures 5, 6, and 7 show no obvious preseismic or coseismic

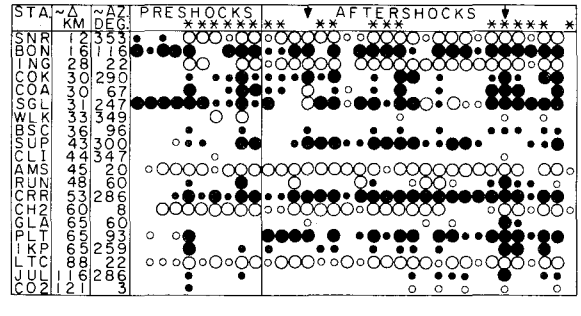

Fig. 19. First motion readings for the events shown in Figures 14 and 15. Open and solid circles same as in Figure 8. Arrows indicate aftershocks for which first motion plots are shown in Figure 20. Asterisks indicate events for which first motions are consistent with pure right-lateral strike-slip motion on a vertical fault plane striking N40°W, the approximate local strike of the Imperial fault.

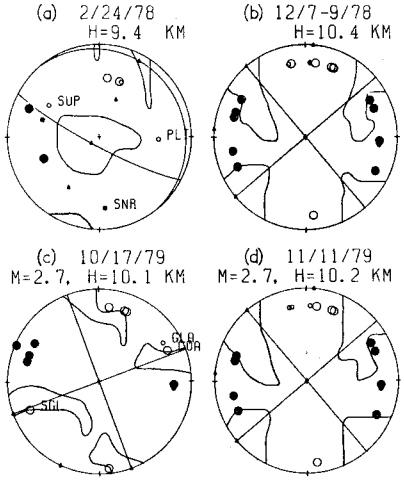

Fig. 20. Lower hemisphere P-wave fault-plane solutions for selected preshocks and aftershocks. (a) Composite for the February 24, 1978, swarm. Hypocenter of 0638 event (Table 3) was used in calculating azimuths and takeoff angles. (b) Composite for the December 7-9, 1978, swarm. Hypocenter for the December 8, 1978, 0847 event (Table 3) was used in calculating azimuths and takeoff angles. (c) Mechanism for aftershock on October 17, 1979, 0937. (d) Mechanism for aftershock on November 11, 1979, 1532. Open and solid circles are as in Figure 8. Slip vectors, compression axes, and tension axes for the solutions shown are indicated by triangles. Contours enclose the locus of positions for slip vectors corresponding to solutions with the minimum number of readings in error. H is depth and M is local magnitude.

changes in frequency content, we decided to perform spectral analysis on them to search for more subtle changes. At least 30 s of record is available in most cases, which makes it possible to look at frequency content of individual phases as well as for the record as a whole. The advantage of knowing the spectra for different parts of the record is that any observed changes in spectra from one event to another can be more easily interpreted. Changes in the attenuation or scattering properties of the medium are likely to affect P and S waves differently [Lockner et al., 1977], and might be especially noticeable in surface-reflected phases such as pP or sP. Frequency changes due to directivity effects would be strongly dependent on azimuth and/or takeoff angle. Changes in stress drop should cause similar frequency changes in all phases at all stations, although spectral content depends to some extent on the details of the stress release [Knopoff and Mouton, 1975].

Figure 21 is a record section illustrating the regional coherence of the three phases that we decided to study. Refraction studies in the Imperial Valley show several kilometers of sedimentary rocks at the surface (P-wave velocities less than 5.65 km/s), underlain by a 'basement' probably composed of metasedimentary rocks (velocities of 5.65-5.85 km/s), which in turn is underlain by a 'subbasement' (velocities greater than 6.6 km/s) inferred to be mafic intrusive rocks [Fuis et al., 1980; McMechan and Mooney, 1980]. Based on this crustal model (Table 1), the P phase is probably a combination of a refracted ray from the subbasement (apparent velocity 7.0 km/s), a direct ray, and turning rays from the basement-subbasement transition. The strong phase that arrives 3 to $3^1/_2$ s later is tentatively identified as pP, but could also be sP. The phase with an apparent velocity of 3.6 km/s is S.

We analyzed frequency content by bandpass filtering the deconvolved seismograms using third-order recursive Butterworth filters [Rader and Gold, 1967]. These filters are computationally efficient approximations to ideal bandpass filters. There are two ways to estimate spectral amplitudes from filtered seismograms. Let s(t) be the seismogram of an arrival beginning at t=0 and let S(f) be its Fourier transform, where t is time and f is frequency. If s(t) is filtered with an ideal bandpass filter in the passband f_1 to f_2, the filtered seismogram $s_f(t)$ is given by

$$s_f(t) = 2\int_{f_1}^{f_2} |S(f)| \cos[\arg[S(f)] + 2\pi ft]\, df$$

Assume that $|S(f)|$ is slowly varying over the range of frequencies $f_1 \le f \le f_2$, such that $|S(f)| \simeq |S(f_o)|$, where $f_o=(f_1+f_2)/2$. Let $\arg[S(f)]=A(f)$ and assume that A(f) can be adequately approximated by a first-order Taylor expansion about f_o:

$$A(f) \simeq A(f_o) + A'(f_o)(f-f_o)$$

With these approximations the integral becomes

$$s_f(t) \simeq 2|S(f_o)|\int_{f_1}^{f_2} \cos[2\pi ft + A(f_o) + A'(f_o)(f-f_o)]\, df$$

Evaluating this integral gives an expression for the filtered arrival:

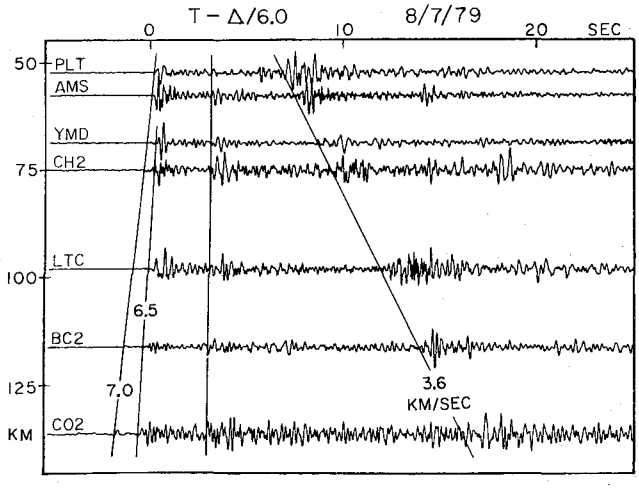

Fig. 21. Seismograms for an M_L 2.5 preshock on August 7, 1979 (Table 2), recorded through modified USGS short-period vertical instruments [Archambeau, 1979].

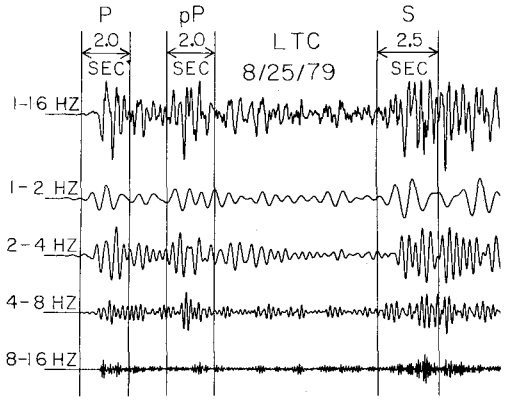

Fig.22. Deconvolved seismogram (top) filtered in four one-octave passbands. Time windows for spectral analysis of P, pP, and S phases are shown.

$$s_f(t) \simeq 2|S(f_o)|(f_2-f_1) \cdot \frac{\sin[(f_2-f_1)(2\pi t + A'(f_o))/2]}{(f_2-f_1)(2\pi t + A'(f_o))/2} \cdot \cos[2\pi f_o t + A(f_o)]$$

Since the filtered arrival is approximately a cosine wave of amplitude $2|S(f_o)|(f_2-f_1)$, modulated by a (sin x)/x function, $|S(f_o)|$ can be estimated by measuring the maximum amplitude of the complex envelope of the filtered data [Farnbach, 1975] and then dividing by $2(f_2-f_1)$. Figure 22 shows a deconvolved seismogram filtered in four one-octave passbands. Since the duration of the impulse response of the filter is inversely proportional to the bandwidth (see expression above), the higher-frequency passbands give better time resolution. Thus, at high frequencies there is often more than one peak within each phase (Figure 22). In such cases, we simply measured the amplitude of the complex envelope of the largest one.

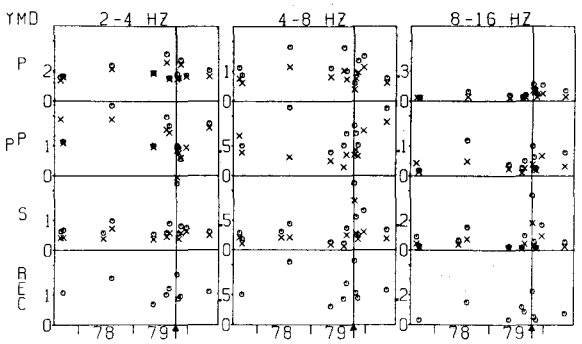

Fig. 23. Spectral amplitudes as a function of time at station YMD for events from the dashed box in Figure 2. Graphs show average spectral amplitudes in the passbands 2-4, 4-8, and 8-16 Hz for the whole record (30 s except for the December 17, 1979, event, starting with the P wave) and for the phases P, pP, and S. All have been normalized to the amplitudes in the passband 1-2 Hz. The crosses are spectral amplitude ratios from envelope amplitudes, and the circles are the ratios from root mean square amplitudes. Vertical lines indicate the time of the Imperial Valley mainshock.

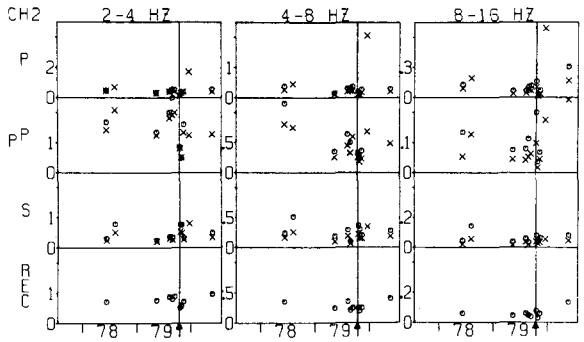

Fig. 24. Spectral amplitudes as a function of time at station CH2 (see Figure 23).

In order to avoid possible problems resulting from the variation in time resolution from one passband to another, we decided to make a second estimate of spectral amplitudes by measuring root mean square amplitudes within time windows 2.0 s long for P and pP and 2.5 s long for S (Figure 22). If, as before, s(t) is a seismogram and S(f) is its Fourier transform, then by Parseval's relationship [Weinberger, 1965, p. 312]

$$\int_{-\infty}^{\infty} |S(f)|^2 \, df = \int_{-\infty}^{\infty} |s(t)|^2 \, dt$$

In the case of the filtered seismogram $s_f(t)$,

$$2\int_{f_1}^{f_2} |S(f)|^2 \, df = \int_{-\infty}^{\infty} |s_f(t)|^2 \, dt$$

If f_o is the center frequency of the passband and $S(f) \simeq S(f_o)$ for $f_1 \leq f \leq f_2$,

$$|S(f_o)| \simeq \sqrt{\frac{1}{2(f_2-f_1)} \int_{-\infty}^{\infty} |s_f(t)|^2 \, dt}$$

For a time series of N samples separated by time ΔT,

$$|S(f_o)| \simeq \sqrt{\frac{N\Delta T}{2(f_2-f_1)}} \sqrt{\frac{1}{N} \sum_{n=1}^{N} |s_f(n\Delta T)|^2}$$

This expression can be used to estimate $|S(f_o)|$ from the root mean square amplitude within a time window.

Figures 23, 24, and 25 show the results of spectral analysis of the records in Figures 5, 6, and 7, respectively. The plots show $|S(f_o)|$ at each station in three passbands as a function of time. These have been normalized to the amplitudes in the lowest-frequency passband used, 1-2 Hz. The crosses are the spectral amplitude ratios from the maximum envelope amplitudes, and the circles are the ratios from the root mean square amplitudes. All of the amplitudes were corrected for noise level by subtracting from

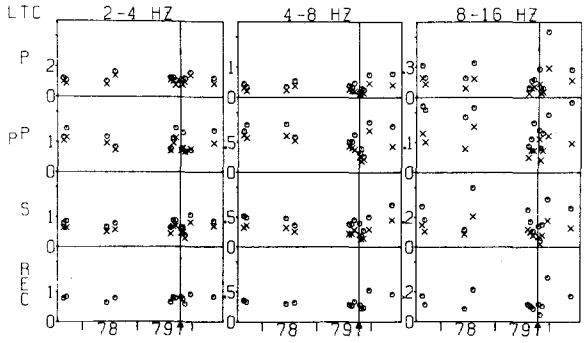

Fig. 25. Spectral amplitudes as a function of time at station LTC (see Figure 23).

each measurement an estimate of the noise amplitude taken from the 6 s of record immediately preceding the P wave. Data for which the signal-to-noise ratio was less than three were not used. The time of the Imperial Valley mainshock is indicated by the arrows and vertical lines on the figures. The rows across correspond to P, pP, S, and the whole record (30 s except for one event, beginning with the P wave). Although there is some scatter, all of the spectral amplitude ratios at all stations are stable with time. Thus, no temporal changes in frequency content from 1-16 Hz are observed for these records.

Several investigators [e.g., Saito and Masuda, 1981; Frankel, 1981a; Archuleta et al., 1982] have presented evidence for a decrease in stress drop with moment for small earthquakes ($M_L < \sim 3$). These studies emphasize the importance of the relationship between event size and spectrum. This relationship is not very obvious in our data when spectral amplitude ratios are plotted versus amplitude in the lowest frequency passband used, 1-2 Hz. We therefore consider the variation in event size to be small enough so that it contributes relatively little to the scatter in Figures 23-25.

The seismograms of events from the second source area studied (Figures 14 and 15) show considerable variation in frequency content, with no overall temporal trends apparent. Within the December 7-9, 1978, swarm, however, seismograms of the later events appear to have more high-frequency energy those of the earlier events. This observation is confirmed by spectral amplitude ratios for the whole record determined by the methods described above. Figure 26 shows these ratios as a function of event number for both preshock swarms. During the December 7-9, 1978, swarm the 8-16 Hz spectral amplitude increased relative to the 1-2 Hz spectral amplitude by about a factor of 3 at both stations CH2 and LTC. (Ratios from YMD are not shown because this station was not operating for most of the preshocks.) The other spectral ratios for this swarm are either stable with time or else show small increases (e.g., 4-8 Hz/1-2 Hz at LTC). Examination of the bandpass filtered records shows that the trends toward higher frequency with time occur over the entire record length. This suggests a systematic increase in stress drop during the December 7-9, 1978, swarm, assuming that simple kinematic source models [Aki and Richards, 1980, chapter 14] are applicable, because the variation in magnitude for these events is small and, in any case, random with time (Table 3). The February 24, 1978, events are clearly enriched in high frequency (4-16 Hz) relative to the December 7-9, 1978, events and show no temporal changes in spectra. These events, however, have predominantly dip-slip mechanisms (Figure 20a) and may not be associated with the Imperial fault, as discussed in the previous section.

In summary, there are no consistent spectral differences between preshocks and aftershocks in the frequency band 1-16 Hz. Thus, we find no evidence for coseismic changes in stress drop or apparent attenuation. During the tightly clustered preshock swarm on December 7-9, 1978, there is some indication of a systematic increase in stress drop. This was not observed for the preshock cluster near the mainshock epicenter. It appears that if there are increases in stress drop due to concentration of stress on unbroken asperities, they are not always observable over these short time periods, even when the events have very similar mechanisms and locations within a few hundred meters. When the events are scattered over even a few kilometers, local heterogeneities in stress and velocity structure could mask this hypothesized effect if it is small. The relatively high-frequency events which preceded the 1971 San Fernando and 1952 Kern County earthquakes began about 2 years before these earthquakes [Ishida and Kanamori, 1978, 1980], so in some cases the detection of changes in average stress drop may require a longer period of observation than was available for this study.

Discussion

We find much stronger evidence to support the prediction of the asperity model regarding waveforms than the prediction about spectra. In particular, the waveform data show that the preshocks of the Imperial Valley earthquake

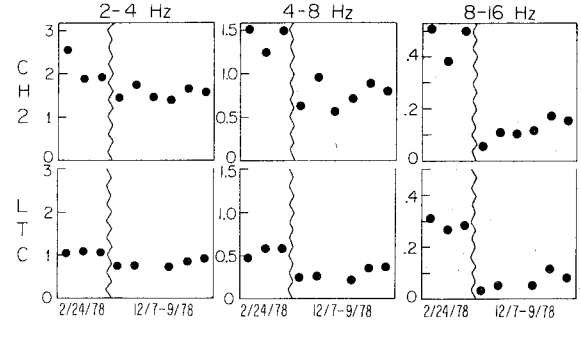

Fig. 26. Spectral amplitudes derived from the root mean square amplitude of the whole record for preshock swarms from dashed box in Figure 3. These have been normalized to the amplitudes in the passband 1-2 Hz. Thirty seconds of record was used in these calculations except for the events noted in the captions for Figures 14 and 15. The effect of the instrument response has not been removed, but is the same for all records.

originated from a relatively small number of highly localized sources in comparison to the aftershocks. This observation can be explained quite well by a version of the asperity model outlined in the introduction. In this model, immediately after a large earthquake the fault surface cannot slip because it is pinned at a large number of geometrical or mechanical irregularities, i.e., the asperities. Small earthquake activity is concentrated along these asperities, which decrease in number as the weaker ones fail under increasing stress. If we assume, for simplicity, that each small earthquake represents the failure of one discrete asperity, then groups of similar earthquakes represent failures of tightly clustered sets of asperities. The larger clusters of asperities might be expected to fail last since they would be stronger than isolated asperities or smaller clusters, other things being equal. However, variations in the loading stress and in the strength and number of asperities are all likely to be important factors in determining the order in which the asperities fail. An alternative interpretation of the waveform data is that each cluster represents one asperity, and the stronger asperities which tend to be the last to fail require more events to completely fracture them. In either case when most, but not necessarily all, of the asperities have broken then the fault becomes unstable and large-scale slip can be triggered by the failure of a critical asperity, as discussed by Brune [1979], Kanamori [1981], and Das and Aki [1977].

Although we did not determine source parameters such as moment and stress drop for these events, standard scaling relations indicate that our conclusions about clustering do not imply unreasonable values for these parameters. Consider the case of the eight preshocks near the mainshock epicenter. From the similarity of waveforms we infer a maximum source separation of 200-400 m. If we assume that these events broke adjacent fault segments without significant overlap of the rupture areas, then the average rupture area per event is either $\pi(200/2)^2/8 = 3.9 \times 10^3$ m^2 or $\pi(400/2)^2/8 = 1.6 \times 10^4$ m^2, depending on which value we take for the maximum separation. This gives an estimated average rupture radius of about 35-70 m. These events have remarkably similar magnitudes, within ±0.2 of M_L 2.4. Applying the empirical moment(M_o)-magnitude relationship of Wyss and Brune [1968] and Thatcher and Hanks [1973],

$$\log M_o = 1.5M_L + 16.0$$

we estimate the moment of these events to be of the order of 4×10^{19} dyne-cm. The stress drop $\Delta\sigma$ for an earthquake of moment M_o on a circular fault of radius r is given by

$$\Delta\sigma = \frac{7}{16}\frac{M_o}{r^3}$$

[Eshelby, 1957; Keilis-Borok, 1959]. Applying this expression, we get a stress drop for these events of approximately 50-400 bars. This is consistent with the results of Hartzell and Helmberger [1982], who estimate an overall stress drop for the mainshock of about 5-10 bars but localized stress drops of about 200 bars.

The calculated depths for both preshocks and aftershocks are concentrated within a surprisingly narrow range: 8-10 km for the southern study area (Figure 2, Table 2) and 9-11 km for the northern area (Figure 3, Table 3). Although the depths of events from south of the border may not be well constrained, the station distribution around the northern study area is reasonably favorable (Figure 19) and nearly all of the locations are quality B, which implies vertical errors of less than 5 km [Lee and Lahr, 1975; Lee et al., 1979]. Furthermore, the depths of several nearby aftershocks determined by P. German (personal communication, 1982) with the aid of arrival times from both temporary and permanent stations are all between 8 and 9 km. These depths agree very well with those in Table 3.

The depths of the preshocks and aftershocks may give some clue as to the nature of the assumed asperities or the distribution of stress. In both areas studied the events are concentrated within the lowermost few kilometers of the basement, which appears to be composed of metamorphosed sedimentary rock. The boundary between the basement and the subbasement, inferred to be mafic intrusive rock, dips about 4°NW along the axis of the Salton Trough [Fuis et al., 1980; McMechan and Mooney, 1980]. One speculative hypothesis is that the asperities are related to irregularities in the basement-subbasement transition zone, which is being offset by the Imperial fault. Another possibility is that the asperities are evenly distributed and the concentration of activity near 10 km is due to a concentration of stress near the depth of the transition from brittle to ductile deformation. This transition is believed to occur near 10 km because this is the approximate depth of the seismic zone in the southern Imperial Valley and also the approximate depth to which faulting during the 1979 Imperial Valley earthquake extended [Hartzell and Helmberger, 1982]. Stresses could be higher near this boundary if basal shear is important as a driving or resistive force. A third possibility is that the 1940 earthquake relieved most of the stress across the upper part of the fault in the regions studied. This would be consistent with the concentration of slip below 5 km in the model of Hartzell and Helmberger [1982] and also the lack of surface faulting near the 1979 epicenter. A more comprehensive study of the depth distribution of earthquakes along the Imperial fault might help to resolve some of these questions.

There is a significant difference between the temporal distribution of the preshocks that we studied near the mainshock epicenter and those 10-12 km north of the border. The preshocks in the southern study area were spread out more or less uniformly over the time period examined, 1977-1979 (Table 2). In contrast, all of the preshocks in the northern study area with strike-slip mechanisms occurred during a 3-day swarm. In the context of the one asperity/ one earthquake model described above, these observations suggest that the asperities in the northern study area were comparatively weak,

because the failure of one asperity apparently triggered the rapid failure of several others close by. The much larger number of aftershocks in the northern study area could also be explained by a tendency toward weaker and/or more numerous asperities there, but may also reflect a deficiency of coseismic slip along that section of fault as suggested by Hartzell and Helmberger [1982].

Although we favor the asperity model as an explanation for the waveform data, there are other models that can account for the change in waveform similarity at the time of the mainshock. Our model is crucially dependent on the assumption that the preshocks and the aftershocks we studied represent slip along the main fault. However, there is evidence that much of the small earthquake activity along the seismogenic zone linking the Imperial fault to the southern end of the San Andreas fault is associated with structures transverse to the trend of this zone and to the Imperial and Brawley faults (Figure 1) [Johnson and Hadley, 1976; Johnson, 1979; Johnson and Hutton, 1980; Hutton and Johnson, 1981]. Earthquake swarms along these transverse structures may be activated by creep events on connecting faults [Johnson and Hadley, 1976; Johnson, 1979]. If these transverse structures also exist along the central portion of the Imperial fault where our study areas are, then some or all of the preshocks and aftershocks could be associated with them. C. Johnson (personal communication, 1982) has suggested that the greater variety of aftershock waveforms could be explained by the simultaneous activation of many different transverse structures by the coseismic and postseismic movement along the Imperial fault. Since our study areas are only a few kilometers long, this hypothesis requires a much higher density of transverse features than can be inferred to exist from the pattern of epicenters in the seismogenic zone to the north.

To help resolve which model best explains the difference between Imperial Valley preshocks and aftershocks, it is important to determine whether normal 'background' seismic activity is more like the aftershocks or the preshocks we studied. Some models, such as Johnson's, suggest that the diversity of small earthquake waveforms after the mainshock is temporary and that background seismicity and preshocks are both characterized by small-scale spatial clustering of successive events. The asperity model predicts in most cases a more gradual change from one waveform pattern to the other during the intervals between large earthquakes. Unfortunately, only a few studies of comparative waveform have been done, and these generally cover short periods of time. One of the more long-term data sets is that of Ishida and Kanamori [1978], who collected Wood-Anderson seismograms recorded at Pasadena for all $M_L<3$ events which occurred within 15 km of the epicenter of the 1971 San Fernando earthquake ($\Delta\sim40$ km) during the period 1961-1971. Master event locations for this region show diffuse seismicity from 1961-1964, quiescence from 1965-1968, and clustering near the eventual hypocenter from 1969-1970. This pattern was confirmed by visual inspection of the waveforms, although Ishida and Kanamori note that it is much more obvious on the EW component than on the NS component. We applied our cross-correlation tests to the hand-digitized records of Ishida and Kanamori. The results are shown in Figures 27 and 28. Because of digitization noise and because only ~9-11 s of record had a large enough amplitude to be digitized in most cases, these cross correlations are not as reliable as those performed with CEDAR data. Nevertheless, Figures 27 and 28 confirm the observations of Ishida and Kanamori that the events during 1961-1964 exhibit a greater variety of waveforms than those during 1969-1970, at least on the EW component. On the EW records, the last four events before the mainshock have very high peak correlations (~0.75), as do the first three events in 1961. Peak correlations between EW seismograms of other pairs of consecutive events are all less than 0.6 (Figure 27). The averages of the NS and EW maximum cross correlations for most of the event pairs are less than 0.6, except for average peak correlations among the last four events, the first three events, and events three through five (Figure 28). These results suggest that tight clustering of hypocenters of consecutive events does not occur very often, even if such clustering is not limited to the time period immediately before large earthquakes. Hence, comparison of waveforms may be a useful tool for monitoring stress conditions along faults.

In summary, we find that preshocks of the 1979 Imperial Valley earthquake occurred in groups of events with strikingly similar waveforms over the entire length of record. The close match in waveform implies similar source mechanisms and clustering of hypocenters within $^1/_4$ wavelength (~$^1/_2$ km) or less. Aftershock waveforms are more variable from one event to the next, although groups of similar events were found during the aftershock period as well. These observations can be explained by the asperity model, which predicts localization of failure on strong, unbroken asperities along the fault during the period preceding moderate to large earthquakes. From our work and that of Ishida and Kanamori [1978] on the 1971 San Fernando earthquake, it appears that this period of enhanced clustering is at least 2-3 years long, but much more work

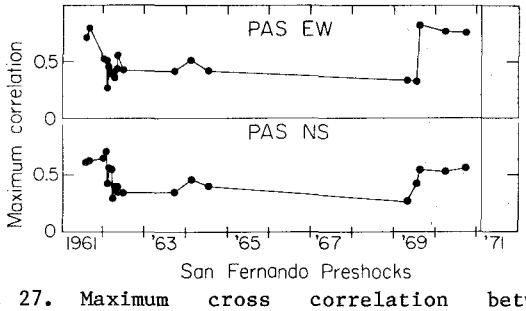

Fig. 27. Maximum cross correlation between seismograms of consecutive events within a 15-km radius of the epicenter of the 1971 San Fernando earthquake, plotted as a function of time. Seismograms are shown in Figs. 2 and 3 of Ishida and Kanamori [1978]. 9-11 s of record were used in most cases, beginning with the S wave. Seismograms were recorded on Wood-Anderson torsion instruments located at Pasadena ($\Delta\sim40$ km).

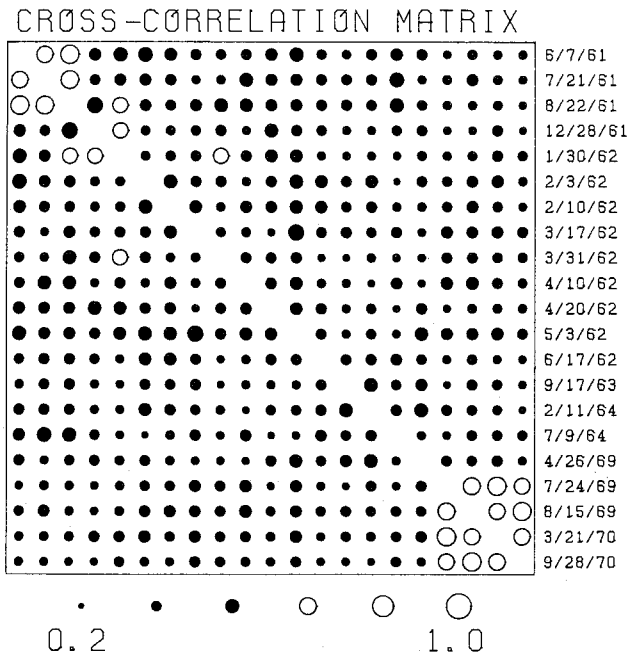

Fig. 28. Complete cross-correlation matrix for events within 15 km of the epicenter of the 1971 San Fernando earthquake. Each circle represents an average of the peak cross correlations determined from the EW and NS Wood-Anderson seismograms recorded at Pasadena (Δ 40 km). See Figure 10 for explanation.

needs to be done to evaluate the significance of this pattern. A second prediction of the asperity model, that of higher stress drop for preshocks, was not in general supported by our data. We did find evidence for increasing stress drop within a tightly grouped set of six preshocks from near the region of maximum surface displacement. However, the frequency content of these events does not differ significantly from that of nearby aftershocks, and no systematic temporal changes in spectra were found for the other preshock cluster we analyzed. It appears that the waveforms of small earthquakes are a more sensitive indicator of seismic potential than are the spectra.

Acknowledgments. We owe special thanks to J. Bernard Minster and Carl E. Johnson, who provided most of the software used in this study and many useful suggestions. We also acknowledge helpful discussions with Stephen Hartzell, Peter German, and Donald Helmberger. Riley Geary and L. K. Hutton assisted us in accessing CEDAR data. Thorough reviews by Peter Molnar, Judith Pechmann, Eugene Humphreys, Luciana Astiz, Edward Corbett, and an anonymous reviewer led to significant improvements in this paper. This research was supported by the U.S. Geological Survey under contracts 14-08-0001-19265 and 14-08-0001-19270, and by the Earth Sciences Section, National Science Foundation grant EAR78-05352. Contribution 3765 of the Division of Geological and Planetary Sciences, California Institute of Technology, Pasadena, California 91125.

References

Aki, K., Characterization of barriers on an earthquake fault, J. Geophys. Res., 84, 6140-6148, 1979.

Aki, K., and P. G. Richards, Quantitative Seismology: Theory and Methods, W. H. Freeman, San Francisco, Calif., 1980.

Archambeau, C. B., Earthquake hazards determinations based on tectonic stress measurements, Semi-Annu. Tech. Rep. 3, U. S. Geol. Surv. Contract No. 14-08-0001-16773, 1979.

Archuleta, R. J., E. Cranswick, C. Mueller, and P. Spudich, Source parameters of the 1980 Mammoth Lakes, California earthquake sequence, J. Geophys. Res., 87, 4595-4607, 1982.

Bakun, W. H., and T. V. McEvilly, Are foreshocks distinctive? Evidence from the 1966 Parkfield and the 1975 Oroville, California sequences, Bull. Seismol. Soc. Am., 69, 1027-1038, 1979.

Brune, J. N., Implications of earthquake triggering and rupture propagation for earthquake prediction based on premonitory phenomena, J. Geophys. Res., 84, 2195-2198, 1979.

Chavez, D., J. Gonzalez, J. N. Brune, F. Vernon, R. Simons, L. K. Hutton, P. T. German, and C. E. Johnson, Mainshock location and magnitude determination using combined U. S. and Mexican data, The October 15, 1979 Imperial Valley Earthquake, U.S. Geol. Surv. Prof. Pap., in press, 1980.

Cipar, J., Broadband time domain modelling of earthquakes from Friuli, Italy, Bull. Seismol. Soc. Am., 71, 1215-1231, 1981.

Das, S., and K. Aki, Fault plane with barriers: A versatile earthquake model, J. Geophys. Res., 82, 5658-5670, 1977.

Ebel, J. E., Evidence for fault asperities from systematic time-domain modelling of teleseismic waveforms, Ph.D. thesis, Calif. Inst. of Technol., Pasadena, 1981.

Eshelby, J. D., The determination of the elastic field of an ellipsoidal inclusion and related problems, Proc. R. Soc. London, Ser. A, 241, 376-396, 1957.

Farnbach, J. S., The complex envelope in seismic signal analysis, Bull. Seismol. Soc. Am., 65, 951-962, 1975.

Frankel, A., Source parameters and scaling relationships of small earthquakes in the northeastern Caribbean, Bull. Seismol. Soc. Am., 71, 1173-1190, 1981a.

Frankel, A., Precursors to a magnitude 4.8 earthquake in the Virgin Islands: Spatial clustering of small earthquakes, anomalous focal mechanisms and earthquake doublets, Eos Trans. AGU, 62, 963, 1981b.

Fuis, G. S., W. D. Mooney, J. H. Healy, G. A. McMechan, and W. J. Lutter, Crustal structure of the Imperial Valley region, The October 15, 1979 Imperial Valley Earthquake, U.S. Geol. Surv. Prof. Pap., in press, 1980.

Geller, R. J., and C. S. Mueller, Four similar earthquakes in central California, Geophys. Res. Lett., 7, 821-824, 1980.

Hamaguchi, H., and A. Hasegawa, Recurrent occurrence of the earthquakes with similar waveforms and its related problems (in

Japanese), J. Seismol. Soc. Jpn., 28, 153-169, 1975.

Hartzell, S., and D. V. Helmberger, Strong motion modelling of the Imperial Valley earthquake of 1979, Bull. Seismol. Soc. Am., 72, 571-596, 1982.

Housner, G. W., Properties of strong ground motion earthquakes, Bull. Seismol. Soc. Am., 45, 197-218, 1955.

Hutton, L. K., and C. E. Johnson, Preliminary study of the Westmoreland, California earthquake swarm, Eos Trans. AGU, 62, 957, 1981.

Imamura, A., Theoretical and Applied Seismology, 358 pp., Maruzen, Tokyo, 1937.

Ishida, M., and H. Kanamori, The foreshock activity of the 1971 San Fernando earthquake, California, Bull. Seismol. Soc. Am., 68, 1265-1279, 1978.

Ishida, M., and H. Kanamori, Temporal variation of seismicity and spectrum of small earthquakes preceding the 1952 Kern County, California earthquake, Bull. Seismol. Soc. Am., 70, 509-527, 1980.

Jennings, C. W., R. G. Strand, T. H. Rogers, M. G. Stinson, J. L. Burnett, J. E. Kahle, R. Streitz, and R. A. Switzer, Fault map of California with locations of volcanoes, thermal springs and thermal wells, Calif. Geol. Data Map Ser., Map 1, Calif. Div. of Mines and Geol., Sacramento, 1975.

Johnson, C. E., I, CEDAR--An Approach to the computer automation of short-period local seismic networks, II, Seismotectonics of the Imperial Valley of southern California, Ph.D. thesis, Calif. Inst. of Technol., Pasadena, 1979.

Johnson, C. E., and D. M. Hadley, Tectonic implications of the Brawley earthquake swarm, Imperial Valley, California, January 1975, Bull. Seismol. Soc. Am., 66, 1133-1144, 1976.

Johnson, C. E., and L. K. Hutton, The 15 October, 1979 Imperial Valley earthquake: A study of aftershocks and prior seismicity, The October 15, 1979 Imperial Valley Earthquake, U.S. Geol. Surv. Prof. Pap., in press, 1980.

Jones, L. M., and P. Molnar, Some characteristics of foreshocks and their possible relationship to earthquake prediction and premonitory slip on faults, J. Geophys. Res., 84, 3596-3608, 1979.

Kanamori, H., The nature of seismicity patterns before large earthquakes, in Earthquake Prediction: An International Review, Maurice Ewing Ser., vol. 4, edited by D. W. Simpson and P. G. Richards, pp. 1-19, AGU, Washington, D. C., 1981.

Kanamori, H., and G. S. Stewart, Seismological aspects of the Guatemala earthquake of February 4, 1976, J. Geophys. Res., 83, 3427-3434, 1978.

Keilis-Borok, V., On estimation of the displacement in an earthquake source and of source dimensions, Ann. Geofis., 12, 205-214, 1959.

Knopoff, L., and J. O. Mouton, Can one determine seismic focal parameters from the far-field radiation?, Geophys. J. R. Astron. Soc., 42, 591-606, 1975.

LeBras, R., A preliminary study for the inversion of strong ground motion data from the 1979 Imperial Valley earthquake, Eos Trans. AGU, 62, 972, 1981.

Lee, W. H. K., and J. C. Lahr, HYPO71 (revised): A computer program for determining hypocenter, magnitude, and first motion pattern of local earthquakes, U.S. Geol. Surv. Open File Rep., 75-311, 1975.

Lee, W. H. K., R. F. Yerkes, and M. Simirenko, Recent earthquake activity and focal mechanisms in the western Transverse Ranges, California, U.S. Geol. Surv. Circ., 799, 1979.

Lockner, D. A., J. B. Walsh, and J. D. Byerlee, Changes in seismic velocity and attenuation during deformation of granite, J. Geophys. Res., 82, 5374-5378, 1977.

McMechan, G. A., and W. D. Mooney, Asymptotic ray theory and synthetic seismograms for laterally varying structures: Theory and application to the Imperial Valley, California, Bull. Seismol. Soc. Am., 70, 2021-2035, 1980.

Mikumo, T., and T. Miyatake, Numerical modelling of space and time variations of seismic activity before major earthquakes, submitted to Geophys. J. R. Astron. Soc., 1982.

Nur, A., Nonuniform friction as a physical basis for earthquake mechanics: A review, Pure Appl. Geophys., 116, 964-991, 1978.

Rader, C. M., and B. Gold, Digital filter design techniques in the frequency domain, Proc. IEEE, 55, 149-171, 1967.

Reyners, M., Long- and intermediate-term precursors to earthquakes--State of the art, in Earthquake Prediction: An International Review, Maurice Ewing Ser., vol. 4, edited by D. W. Simpson and P. G. Richards, pp. 333-347, AGU, Washington, D. C., 1981.

Rial, J. A., The Caracas, Venezuela earthquake of July, 1967: A multiple source event, J. Geophys. Res., 83, 5405-5414, 1978.

Richter, C. F., Elementary Seismology, 768 pp., W. H. Freeman, San Francisco, Calif., 1958.

Saito, K., and T. Masuda, Precursory change of spectral characteristics before the 1978 Miyagiken-oki earthquake, Sci. Rep. Tohoku Univ., Ser. 5, 27, 95-109, 1981.

Sharp, R. V., Surface faulting in Imperial Valley during the earthquake swarm of January-February, 1975, Bull. Seismol. Soc. Am., 66, 1145-1154, 1976.

Spieth, M. A., and R. J. Geller, Precise relative locations of local earthquakes near San Juan Bautista, California, Eos Trans. AGU, 62, 958, 1981.

Stauder, W., and A. Ryall, Spatial distribution and source mechanism of microearthquakes in Central Nevada, Bull. Seismol. Soc. Am., 57, 1317-1345, 1967.

Thatcher, W., and T. C. Hanks, Source parameters of southern California earthquakes, J. Geophys. Res., 78, 8547-8576, 1973.

Thatcher, W., J. A. Hileman, and T. C. Hanks, Seismic slip distribution along the San Jacinto fault zone, southern California, and its implications, Geol. Soc. Am. Bull., 86, 1140-1146, 1975.

Tsujiura, M., The difference between foreshocks and earthquake swarms, as inferred from the similarity of seismic waveform (in Japanese),

Bull. Earthquake Res. Inst., Tokyo Univ., 54, 309-315, 1979a.

Tsujiura, M., Mechanism of the earthquake swarm activity in the Kawanazaki-oki, Izu Peninsula, as inferred from the analysis of seismic waveforms, Bull. Earthquake Res. Inst., Tokyo Univ., 54, 441-462, 1979b.

Tsumura, K., I. Karakama, I. Ogino, and M. Takahashi, Seismic activities before and after the Izu-Oshima-Kinkai earthquake of 1978 (in Japanese), Bull. Earthquake Res. Inst., Tokyo Univ., 53, 675-706, 1978.

Wallace, T. C., D. V. Helmberger, and J. E. Ebel, A broadband study of the 13 August 1978 Santa Barbara earthquake, Bull. Seismol. Soc. Am., 71, 1701-1718, 1981.

Weinberger, H. F., A First Course in Partial Differential Equations, 446 pp., Xerox College Publishing, Lexington, Ky., 1965.

Wu, F. T., Strength of fault zone materials above 15 km depth and tectonic stresses, in Proceedings of Conference IX, Magnitude of Deviatoric Stresses in the Earth's Crust and Upper Mantle, vol. II, U. S. Geological Survey, Menlo Park, Calif., 1980.

Wyss, M., and J. N. Brune, The Alaska earthquake of 28 March 1964: A complex multiple rupture, Bull. Seismol. Soc. Am., 57, 1017-1023, 1967.

Wyss, M., and J. N. Brune, Seismic moment, stress, and source dimensions for earthquakes in the California-Nevada Region, J. Geophys. Res., 73, 4681-4694, 1968.

(Received March 26, 1982;
revised July 30, 1982;
accepted September 3, 1982.)